HOKKAIDO UNIVERSITY

Title	Fluctuation of Time-Resolved X-ray Diffraction Reveals the Rotational Dynamics of Nanoparticles in Polymer Materials
Author(s)	Arai, Tatsuya; Kuramochi, Masahiro; Mio, Kazuhiro et al.
Citation	Nano letters, 25(38), 14156-14165 https://doi.org/10.1021/acs.nanolett.5c03840
Issue Date	2025-09-24
Doc URL	https://hdl.handle.net/2115/98113
Rights	This document is the Accepted Manuscript version of a Published Work that appeared in final form in Nano letters, copyright © American Chemical Society after peer review and technical editing by the publisher. To access the final edited and published work see https://pubs.acs.org/articlesonrequest/AOR-9CGGMK3UYHRBNGYQIEUW Articles on Request author-directed link.
Type	journal article
File Information	20250911_DXB_polymers_Nanoletters4_rev3.pdf

Hokkaido University Collection of Scholarly and Academic Papers : HUSCAP

Fluctuation of time-resolved X-ray diffraction reveals the rotational dynamics of nanoparticles in polymer materials

Tatsuya Arai[1], Masahiro Kuramochi[2,3], Kazuhiro Mio[4,5], Hiroshi Sekiguchi[6], Sakae Tsuda[1], Daisuke Sasaki[3], Tomoyasu Aizawa[1], and Yuji C. Sasaki[3,4]*

1 Graduate School of Life Science, Hokkaido University, Sapporo, 060-0810, Japan

2 Graduate School of Science and Engineering, Ibaraki University, Hitachi, 316-8511, Japan

3 Graduate School of Frontier Sciences, The University of Tokyo, Kashiwa, 277-8561, Japan.

4 AIST-UTokyo Advanced Operando Measurement Technology Open Innovation Laboratory, National Institute of Advanced Industrial Science and Technology, Kashiwa, 277-0882, Japan.

5 Graduate School of Medical Life Science, Yokohama City University, Yokohama 230-0045, Japan.

6 Diffraction and Scattering Division, Japan Synchrotron Radiation Research Institute, Sayo gun, 679-5198, Japan.

*Corresponding author: Tatsuya Arai

KEYWORDS

X-ray diffraction, diffracted X-ray blinking, nanoparticle, polymer nanocomposite,

ABSTRACT

Polymer nanocomposites, consisting of a polymer matrix and nanoparticles, are key materials in modern soft matter science. Because their macroscopic properties are closely linked to nanoscale dynamics, developing techniques to observe nanoparticle motion is essential. Here, we present novel methods to analyze rotational dynamics of crystalline nanoparticles in various polymers using conventional time-resolved X-ray diffraction (TR-XRD). In the first approach, diffraction intensity fluctuations caused by nanoparticle rotation were analyzed via autocorrelation functions to extract relaxation times—defined as the duration for a diffraction spot to traverse a single pixel of detector. The relaxation times varied significantly depending on the material's rigidity and temperature. Secondly, two-time correlation analysis applied to TR-XRD data revealed time-dependent changes in nanoparticle dynamics during polymer phase transitions. These methods expand the utility of TR-XRD beyond structural analysis, offering a powerful tool to probe nanoscale rotational motion across a wide range of materials, from liquids to solids.

Nanoparticles (NPs) dispersed in polymer matrices not only serve as functional fillers that enhance mechanical [1], electrical [2], and thermal [3] properties of composite materials, but also act as sensitive tracers to monitor polymer dynamics in situ [4]. NP motion in polymer nanocomposites (PNCs) results from local interactions such as entanglement, confinement, and interfacial adhesion. This nanoscale dynamic behavior is closely linked to bulk properties such as viscoelasticity, stiffness, and responsiveness to external stimuli. Therefore, understanding NP dynamics within the polymer matrix is essential for understanding, predicting, and controlling the physical property of PNCs. So far, a variety of experimental techniques have been developed to investigate the dynamics of NPs. Among them, single-particle tracking (SPT) [5] and photon correlation methods [6] are especially effective and complementary for probing dynamic across different length and time scales. SPT enables the direct observation of individual particle trajectories over time. This technique is particularly useful in heterogeneous media, where particles may experience spatially varying constraints or interactions, although it has limitations in spatial and temporal resolution. In contrast, photon correlation techniques—such as dynamic light scattering (DLS) [7], fluorescence correlation spectroscopy (FCS) [8], and X-ray photon correlation spectroscopy (XPCS) [9–11],—provide ensemble-averaged insights into particle motion by analyzing temporal fluctuations in scattered or emitted light. These methods are highly sensitive to collective dynamics and are applicable across a wide range of length and time scales. However, these methods primarily visualize translational dynamics but do not capture rotational dynamics, which limits our understanding of how particle rotation relates to the macroscopic viscoelasticity of materials. Therefore, there is a strong demand for a versatile method to measure the real-time rotational dynamics of NPs, which would offer a deeper understanding of particle

behavior in viscoelastic environments and contribute to the development of advanced functional materials.

Diffracted X-ray blinking (DXB) is a method originally proposed to monitor the rotational motion of protein molecules anchored on a substrate [12–15]. In this method, protein molecules fixed on a substrate are labeled with nanocrystals and are exposed to a monochromatic X-ray beam and its time-resolved X-ray diffraction images are recorded. Information of the rotational dynamics of protein molecules is extracted from the fluctuation of the X-ray diffraction intensity by using an autocorrelation function (ACF). Recently, this method was applied to other than proteins such as grain motion of silver halide during photolysis chemical reaction [16], surface dynamics of crystalline polymer [17], and dynamics of carbon black and polybutadiene in rubber materials [18]. However, detailed rotational dynamics of NPs in various polymers and their temperature-dependence have not been investigated with DXB.

Here, we applied the DXB method to monitor the rotational motion of ZnO particles (diameter = 80–200 nm) in six different polymer samples: polycaprolactone (PCL), vulcanized natural rubber (vNR), 2.8% PVA (polyvinyl alcohol)–borax hydrogel, 3.6% PVA–borax hydrogel, 70% PEG1500 solution, and PEG600. ZnO was chosen as a probe for DXB because of its inexpensiveness and good crystallinity. Time-resolved X-ray diffraction measurements for the six samples were performed at beamline BL-40XU of SPring-8, as shown in Fig. 1A. The sample, either contained in a polyimide film tube (φ = 1 mm) or prepared as a sheet (1 mm thick), was exposed to a monochromatic X-ray beam (λ = 1.0Å), and its diffraction pattern was recorded with different time resolutions depending on samples (Fig. 1B, Table S1). Fig. 1C shows time-averaged X-ray diffraction pattern of the 70% PEG1500 containing ZnO NPs at 25°C and Fig. 1D shows corresponding 1D-conveted X-ray diffraction pattern. A broad halo pattern derived from 70%

PEG1500 solution and several Debye-Scherrer rings derived from (100) to (201) planes of ZnO NPs were observed around 2θ = 16° and at 2θ = 20°–43°, respectively. The concept of the DXB method is described as follows (and also shown in supporting information Fig. S1): When an X-ray beam is scattered by a sample containing many crystalline particles, a Debye-Scherrer ring is observed, which is composed of scattered diffraction spots derived from the crystallites that fulfill the Brag's low ($2d\sin\theta = n\lambda$). If the angular position of particles is stable during the exposure time, a diffraction intensity distribution of the ring is "fixed". On the other hand, if particles in the sample undergo rotational dynamics during the exposure time, this diffraction intensity distribution will change accordingly, which is observed as "blinking" on the narrow ring, due to the limited 2θ-angle range defined by Bragg's law. Figure 1E and Movie S1 show the blinking behavior of X-ray diffraction from ZnO NPs in 70% PEG1500 solution, where numerous diffraction spots repeatedly appear and disappear, resulting in fluctuations in diffraction intensity. The concept of DXB is to track these intensity fluctuations over time applying an autocorrelation function (ACF) of the time-course of the diffraction intensity at each pixel (Fig. 1F and S2):

$$G(\tau) = \frac{\langle I(t)I(t+\tau)\rangle}{\langle I(t)\rangle^2} \quad [1]$$

, where *I(t)* is the diffraction intensity at a pixel, brackets < > means time average, and τ is lag time. The ACF curve was calculated by varying τ from 0 to half of total exposure time and was fitted to an exponential function:

$$Fit(\tau) = Aexp(-\Gamma\tau)^{\gamma} + 1 \quad [2]$$

, where A is the amplitude, Γ is the decay constant (= 1/relaxation time; τ_R), and γ is a stretch rate of the exponential (usually 1 for the rotational Brownian motion). If the particles exhibit complex rotational dynamics, employing more advanced fitting approaches, such as multi-exponential functions, could yield a more comprehensive characterization. The relaxation time τ_R represents the average time, during which a diffraction spot passes through one pixel of the detector (75 μm × 75 μm), providing a measure of the rotational speed of the particles in the sample. It should be noted that the effect of translational motion of NPs in this experiment can be neglected (as shown in Fig. S3), indicating that the observed blinking originates solely from their rotational dynamics.

The rotational dynamics of ZnO NPs in the six different polymeric materials at 25°C were evaluated by the ACF analysis for 1-pixel intensity fluctuations across all observed crystalline planes. Fig. 2A shows the median of the normalized ACF curves ((G(τ)−1)/A), where a faster decay of the curve indicates faster rotational motion of the ZnO NPs. The distribution of τ_R obtained by fitting with a single exponential function (Eq. [2]) is shown as a logarithmic histogram in Fig. 2B. This single-pixel analysis technique enables the characterization of rotational dynamics distributions across tens of thousands of pixels. The τ_R distribution on a logarithmic scale exhibited a clear Gaussian profile (black dashed line) in all samples, with peak positions closely matching their respective median values (Fig. S4). The relaxation time τ_R of all samples exhibits an approximately one-order-of-magnitude spread, which could be attributed not only to the inherent randomness of rotational Brownian motion but also to the particle size distribution (80–200 nm). For example, because the rotational diffusion coefficient scales inversely with the cube of the particle radius, an 80 nm particle would rotate roughly 16 times faster than a 200 nm particle. The τ_R for the six samples varied over four orders of magnitude, in the following order: PCL > vNR > 3.6% PVA-borax hydrogel > 2.8% PVA-borax hydrogel > 70% PEG1500 solution > 100%

PEG600. This trend is consistent with the rigidity of each sample, suggesting the validity of the DXB analysis. Slower dynamics were observed in the solid materials PCL and vNR, with relaxation times of 5.16×10^{1} sec and 1.02×10^{1} sec, respectively. In PVA-borax hydrogels, which behave as liquid-like gels at 25°C, the τ_R decreased by approximately two orders of magnitude (1.07×10^{-1} sec for 3.6% and 6.95×10^{-2} sec for 2.8%) compared to the solid materials. Because the range of rotational fluctuation detectable by DXB is very small (e.g., <0.03°), rotational dynamics of particles even in such solid and gel materials can be observed. On the other hand, due to such high angular resolution, capturing fast rotational dynamics requires diffraction measurements with extremely high temporal resolution. For example, the τ_R of 70% PEG1500 solution and liquid PEG600 were 1.21×10^{-2} sec and 2.68×10^{-3} sec, which approach near the time-resolution limit of the detector used in this study (3.33×10^{-4} sec), suggesting that particle dynamics in low-viscosity liquids such as water cannot be observed under the current experimental conditions.

To evaluate the temperature-dependent rotational dynamics of NPs in PNCs, we applied DXB to ZnO NPs in five of the six samples at different temperatures (Table S1). Time-average X-ray diffraction patterns of 70% PEG1500 solution measured at 25°C, 5°C, and –15°C exhibited almost same (Fig. 3A and S5), although the ACF curves calculated from intensity fluctuations of ZnO exhibited clear temperature dependence, decaying more slowly at lower temperatures and more quickly at higher temperatures (Fig. 3B). The distribution of the ACF relaxation time fitted with an exponentially modified Gaussian distribution (Fig. 3C) showed the median value of 70% PEG1500 was the fastest at 25°C (1.21×10^{-2} sec) and it gradually increased with decreasing the temperature, reaching 2.65×10^{-2} sec at –15°C. This result suggests that the rotational dynamics of NPs in 70% PEG1500 solution scale with temperature, although the dependence is relatively

weak because the sample remained in a liquid state across in entire temperature range [19]. On the other hand, in the case of 2.8% PVA-borax hydrogels, the τ_R elongated significantly with decreasing the temperature (3.72×10^{-2} sec at 50°C and 2.07×10^{-1} sec at 0°C, in Fig 3B and C). This behavior would reflect the strong temperature dependence of the physical and mechanical properties of PVA–borax hydrogels [20] (Fig. S6). The gel became more flexible at higher temperatures, allowing the ZnO NPs to rotate more freely. In contrast, it stiffened at lower temperatures, trapping the NPs within the matrix and thereby suppressing their rotational motion. In PEG600, the τ_R was 2.68×10^{-3} sec at 25°C but it increased markedly to 2.47×10^{-1} sec at 5°C. This dramatic change is likely due to crystallization of PEG600, as the broad halo pattern (2θ = 12°–16°) characteristic of amorphous PEG600 observed at 25°C decreased in intensity of the XRD, while two strong diffraction peaks at 2θ = 12.5° and 15.5°, corresponding to crystalline PEG600, emerged at 5°C (Fig. 3A, right). This liquid–solid phase transition led to a two-order-of-magnitude reduction in the rotational dynamics of the ZnO NPs. At –15°C, the τ_R was further increased to 5.11×10^{-1} sec, reflecting increased crystallinity of PEG600; the NPs were strongly trapped within the crystallized PEG600. Fig. 3D shows the summarized relaxation time τ_R vs temperature of ZnO NPs in various polymeric materials (original data was shown in Fig. S7). In all materials, a clear temperature dependence was observed, indicating enhanced rotational mobility of the NPs at higher temperature due to reduced viscosity or increased flexibility of the polymer matrix, while restricted rotational motion was observed at lower temperatures, caused by increased viscosity, polymer stiffening, or crystallization effects, depending on the specific material. These results suggest that this temperature-dependent DXB method will provide insight into local viscoelasticity as rotational dynamics are sensitive to the local micro-viscosity.

To evaluate potential X-ray-induced radiation damage to the samples, which can progressively accelerate the dynamics [21], we applied the two-time correlation (TTC) analysis [22] to the diffraction intensities of our samples (Fig. 4A, B). TTC analysis is often used in XPCS to evaluate the change of the dynamics during the measurement [23]. The TTC analysis for this study was applied to the time series of diffraction intensities from all observable planes of ZnO by using

$$C(t_1, t_2) = \frac{\langle \delta I(t_1) \delta I(t_2) \rangle_p}{\langle I(t_1) \rangle_p \langle I(t_2) \rangle_p} \quad [3]$$

, where t_1 and t_2 indicate the two selected times, $\delta I(t) = I(t) - \langle I \rangle$, and $\langle \rangle_p$ indicates the average over all pixels across all observed crystalline planes. The resulting $C(t_1, t_2)$ was visualized as a heatmap where the lower left and upper right corners represent the beginning and end of the measurement, respectively (Fig. 4A). In this analysis, the $C(t_1, t_2)$ value reflects the correlation of diffraction intensity patterns between images taken at different times, indicating the similarity of the overall angular orientations of all exposed ZnO NPs. When the time lag between t_1 and t_2 is small, the value of $C(t_1, t_2)$ is high. As the lag increases, $C(t_1, t_2)$ gradually decreases, and this relaxation time should remain constant if the rotational dynamics of the NPs are time-invariant (Fig. 4A, right).

The TTC of 70% PEG1500 solution at different temperatures exhibited a strong temperature dependence. The decay of $C(t_1, t_2)$ with increasing lag time became slower at lower temperatures. To quantify the damage to the sample, we extracted diagonal cuts from the TTC map along different lag times ($\tau = t_1 - t_2$) as indicated by colored arrows. It showed no monotonic increase or decrease over time, suggesting minimal beam-induced damage. This is further supported by the stable intensity fluctuations observed in the halo region (Fig. S8). The increase

in intensity is only about 1%, and such a small change is more likely due to fluctuations of the synchrotron light source rather than beam-induced damage, confirming that the samples remained undamaged during X-ray exposure. The TTC heatmaps for the other samples were shown in Fig. S9, also showing no dramatic change in dynamics during the X-ray exposure period.

During phase transition in polymeric materials, such as crystallization, molecular dynamics of polymer molecules can change dramatically. To monitor such changes, we applied DXB-based TTC analysis to ZnO NPs in PEG600 undergoing a phase transition, for which we conducted time-resolved X-ray diffraction measurements while gradually cooling or heating (0.1 °C/s). In this measurement, the time resolution was set to 40 ms/frame to match the slow cooling rate. Fig. 5A-C compares the TTC and the corresponding time-resolved X-ray diffraction heatmaps. Upon cooling, PEG600 was crystallized at 140 sec corresponding to 11°C and was completed at 240 sec corresponding to 1°C (Fig. 5A). Blinking of the ZnO X-ray diffraction during this process was visualized in Fig. 5B, showing that it gradually slowed down as the temperature decreased. In the TTC map (Fig. 5C), the TTC before crystallization (stage (i)) appeared as a diagonal line along $t_1 = t_2$ with almost no width, indicating that the rotational motion of ZnO particles was too fast to be captured at the current frame rate. This result is corresponding to the result in Fig. 2 where the τ_R of PEG600 at 25°C was 2.68 ms. At the onset of crystallization (stage (ii)), the relaxation time in the TTC map increased, indicating a significant slowdown in the rotational motion of the ZnO particles, likely due to their entrapment within the forming PEG600 crystalline matrix. However, in stage (ii), the relaxation time did not increase linearly despite the decreasing temperature and this trend continued until 240 sec (corresponding to 1°C). After crystallization was complete, the relaxation time continued to increase gradually, indicating the rotational dynamics of the ZnO NPs gradually slow down. On the other hand, such two-step process was not observed during melting

(from –15°C to 25°C) and NP dynamics was gradually increased with increasing the temperature (Fig. 5C and S10). This two-step phase-transition during cooling is consistent with the previous report, where the low-molecular-weight PEGs (below PEG1000) exhibited a two-step crystallization process: an initial slow crystallization at higher temperature followed by a rapid crystallization at lower temperature [24]. As the crystals grew slowly at the initial crystallization process (stage (ii)), ZnO NPs may have been continuously displaced, preventing a sharp drop in nanoparticle dynamics (Fig. 5D). After reaching the second crystallization (stage (iii)), the rotational dynamics of ZnO NPs trapped in PEG600 matrix continued to slow due to reduced thermal energy and increased matrix rigidity. These results clearly demonstrate that DXB combined with TTC analysis can effectively capture NP dynamics during a polymer phase transition. Similar dynamic behaviors during phase transition of polymeric materials have previously been observed using XPCS. For example, Hoshino et al. visualized the curing process of epoxy resins containing SiO_2 probe particles with XPCS [25,26]. DXB, using crystalline probe particles, offers an alternative to XPCS for monitoring dynamic changes of variety of polymer systems.

In this study, the DXB method was applied as a novel X-ray-based method to monitor the rotational dynamics of NPs in various polymer systems (Fig. 2). Particle dynamics in polymers have traditionally been investigated using optical techniques such as SPT, XPCS, DLS, and FCS [27,28]. Compared to these methods, DXB offers three main advantages: (i) it directly measures rotational diffusion with high angular resolution, but not translational diffusion, (ii) it can selectively analyze specific types of particles, even in PNCs containing multiple types of NPs of similar sizes [29], and (iii) it imposes no limitation on size of target particles, as long as they are sufficiently large to produce well-defined diffraction spots. Among the above techniques, XPCS

is the most closely related to DXB. XPCS utilizes coherent X-rays to capture fluctuations in speckle patterns in small-angle X-ray scattering, enabling analysis of translational and rotational dynamics of particles across a wide size range under appropriate conditions [30,31]. However, XPCS always requires a highly coherent X-ray beam, which limits its application to specific beamlines at synchrotron radiation facilities. In contrast, DXB does not require coherent X-rays and can be performed using standard synchrotron or even laboratory-based X-ray sources [13].

Another advantage of the DXB method is that it can be easily optimized or combined with other techniques. For example, when DXB is combined with grazing-incidence (GI) X-ray diffraction, it enables observation of the rotational dynamics of NPs specifically in the near-surface region [17]. Although such measurement has been performed with XPCS as GI-XPCS [32], it should note again that DXB does not require a coherent X-ray beam from a synchrotron facility. Another optimization for DXB is using a polychromatic X-ray source instead of monochromatic one. As defined by Bragg's law ($2d\sin\theta = n\lambda$), employing a polychromatic X-ray beam with a high bandwidth increases the observable 2θ range for diffraction spots. As a result, diffraction spots derived from crystalline objects exhibit longer lifetimes in 2θ-direction, appearing as moving particles on a detector that can be tracked. This technique is known as diffracted X-ray tracking (DXT) [33], and it has been used to evaluate the rotational motion of NP-labeled protein molecules. When applied to PNCs, DXT can provide more detailed insight into the NP dynamics.

While DXB provides a powerful tool to probe the rotational dynamics of crystalline NPs, it has certain limitations. For example, when the sample contains too many particles, the contrast of X-ray diffraction intensity fluctuations can be buried in noise, which arises from factors such as crystallinity, beam size, camera distance, and polymer composition. Under our experimental conditions, however, a ZnO nanoparticle concentration of 10 mg/mL provided sufficient contrast.

To reduce noise and increase contrast, reducing the beam size, particle concentration, or sample thickness can help maintain well-defined diffraction spots. In addition, when the sample contains a large number of particles, the measured intensity fluctuations are effectively dominated by the larger particles within the distribution, since larger NPs scatter X-rays more strongly.

In DXB analysis, the relaxation time τ_R reflects the average duration of a diffraction spot passing through a detector pixel and is influenced by both nanoparticle dynamics and experimental factors, such as camera distance, diffraction spot size, and sample thickness. Therefore, τ_R cannot be directly converted into quantitative parameters such as the rotational diffusion coefficient based on the present data. Establishing such a conversion will require systematic measurements on Newtonian fluids (e.g., a glycerol–water mixture) under various conditions. In addition, experimental X-ray diffraction data for samples (e.g., ZnO nanoparticle powder) rotated at precisely controlled angular velocities, as well as simulated diffraction patterns based on known particle sizes, shapes, and rotational behaviors can be helpful. DXB analysis for these datasets would allow us to establish the correlation between the relaxation time τ_R and the rotational diffusion coefficient.

In conclusion, we have succeeded in measuring the material- and temperature-dependent rotational dynamics of ZnO NPs in several polymers by analyzing the image sequence of the time-resolved X-ray diffraction. Furthermore, we combined DXB and TTC analysis for the first time, enabling real-time monitoring of NP dynamics during phase transitions in PEG. This approach holds promise for in situ investigations of nanoparticle behavior under environmental changes such as temperature variation, electric fields, or mechanical stress, using crystalline particles as sensitive probes.

FIGURES

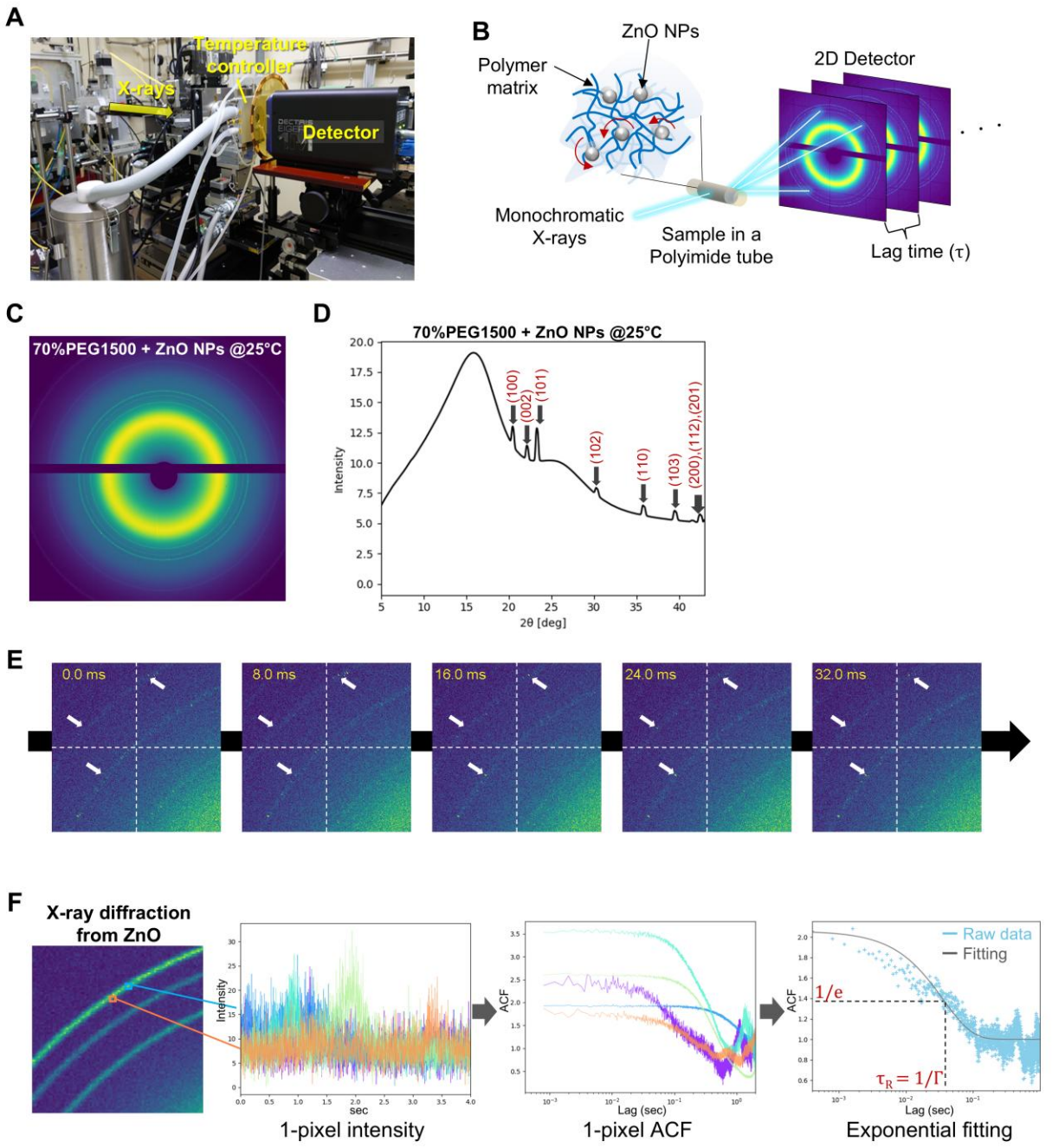


Figure 1. DXB analysis for NPs in polymers. (A) Experimental setup at beamline BL40XU, SPring-8. (B) Schematic illustration for the time-resolved X-ray diffraction measurement for

polymeric samples. A monochromatic X-ray beam was directed to sample containing ZnO particles, and time-resolved X-ray diffraction images were recorded. (C) Time-averaged X-ray diffraction image of the 70% PEG1500 solution containing ZnO NPs. (D) Corresponding 1D X-ray diffraction profile converted from (C). (E) Representative time-course of the X-ray diffraction pattern showing the diffracted X-ray blinking. Arrows indicate the appearance ("in") and disappearance ("out") of bright X-ray diffraction spots. (F) DXB analysis procedure. The time-course of diffraction intensity was extracted for each pixel and analyzed using ACF, followed by exponential fitting to determine the relaxation time (τ_R) for each curve.

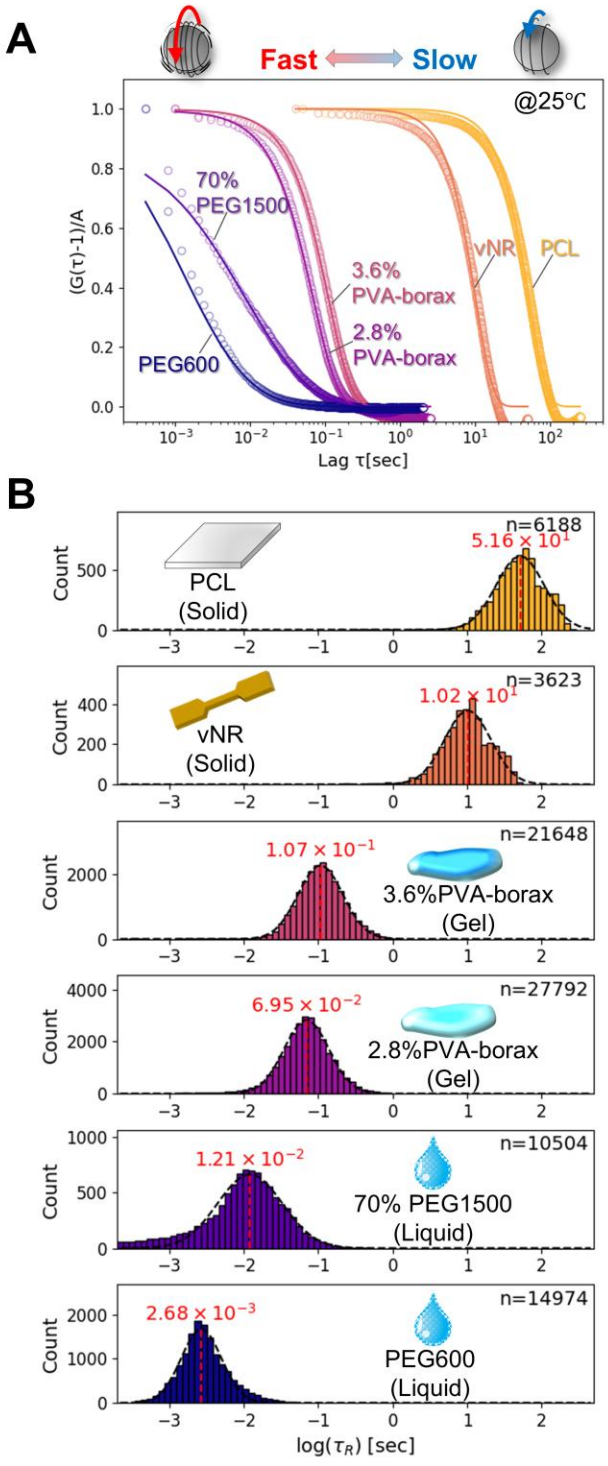


Figure 2. DXB analysis results for ZnO NPs in six different polymeric materials at 25°C. (A) Median values of normalized ACF curves ((G(τ) – 1)/A), representing the rotational dynamics of

NPs. Median values are shown as open circles, and their exponential fits ($Fit(\tau) = Aexp(-\Gamma\tau)^{\gamma} + 1$) are shown as solid lines. (B) Histograms showing the relaxation time distributions of the six samples on a logarithmic scale. Each histogram was fitted with a gaussian function (black dashed line), and the relaxation time at the peak was indicated in red. n indicates the number of pixels used in the analysis.

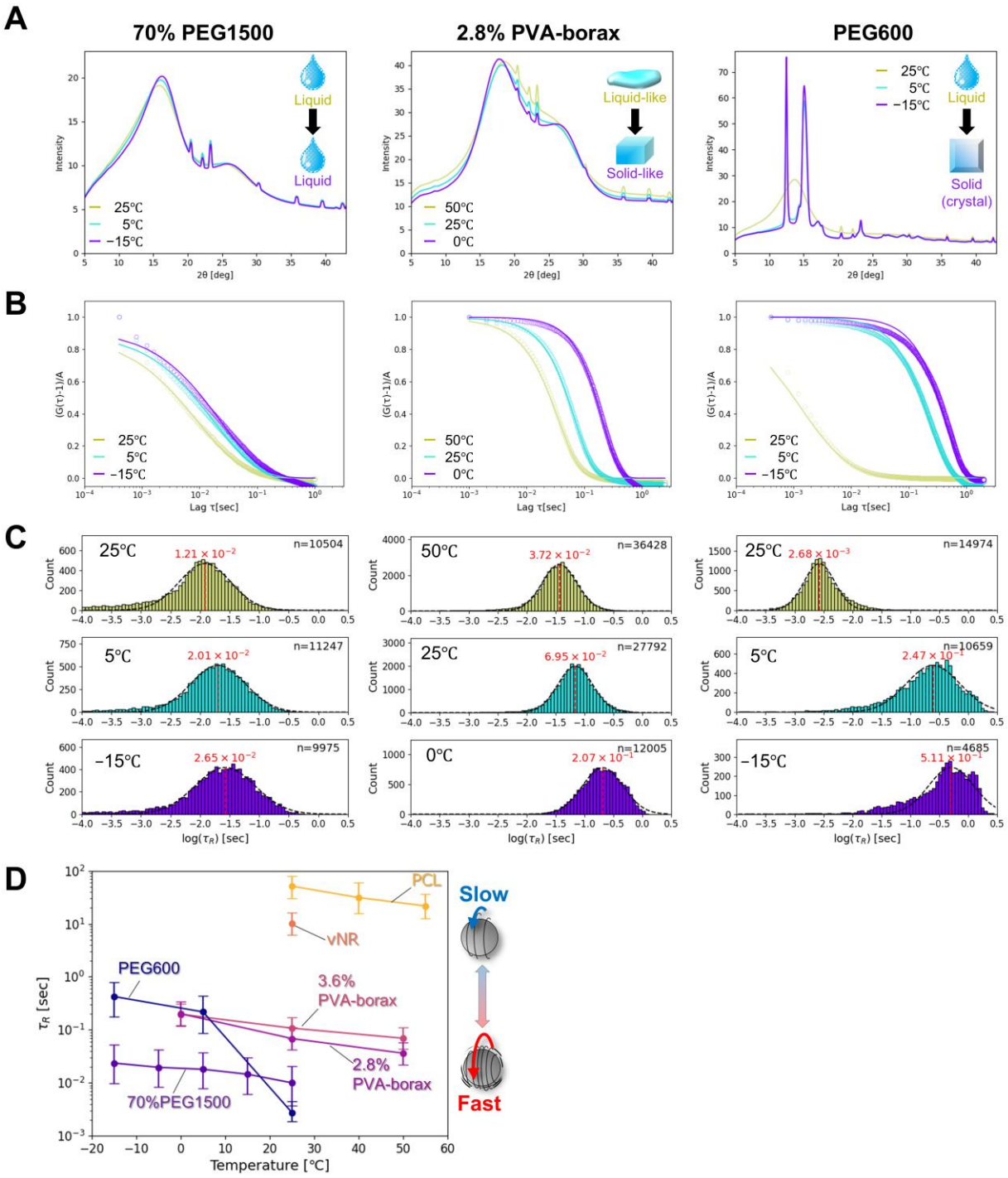


Figure 3. DXB analysis results for ZnO NPs in 70% PEG1500 and 2.8% PVA-borax hydrogel, and PEG600 at different temperatures. (A) Comparison of converted 1D X-ray diffractions at different temperatures. (B) Median values of normalized ACF curves ((G(τ) – 1)/A), representing

the rotational dynamics of NPs. Median values are shown as open circles, and their exponential fits ($Fit(\tau) = Aexp(-\Gamma\tau)^{\gamma} + 1$) are shown as solid lines. (C) Histograms showing the relaxation time distributions of the six samples on a logarithmic scale. Each histogram was fitted with a Gaussian function (black dashed line), and the relaxation time at the peak was indicated in red. n indicates the number of pixels used in the analysis. (D) Temperature dependence of the relaxation time (τ_R) of ZnO nanoparticles in different polymeric materials. The median values of relaxation time τ_R was plotted against temperature (°C) for each sample. Error bars represent the first and third quartiles of the distribution.

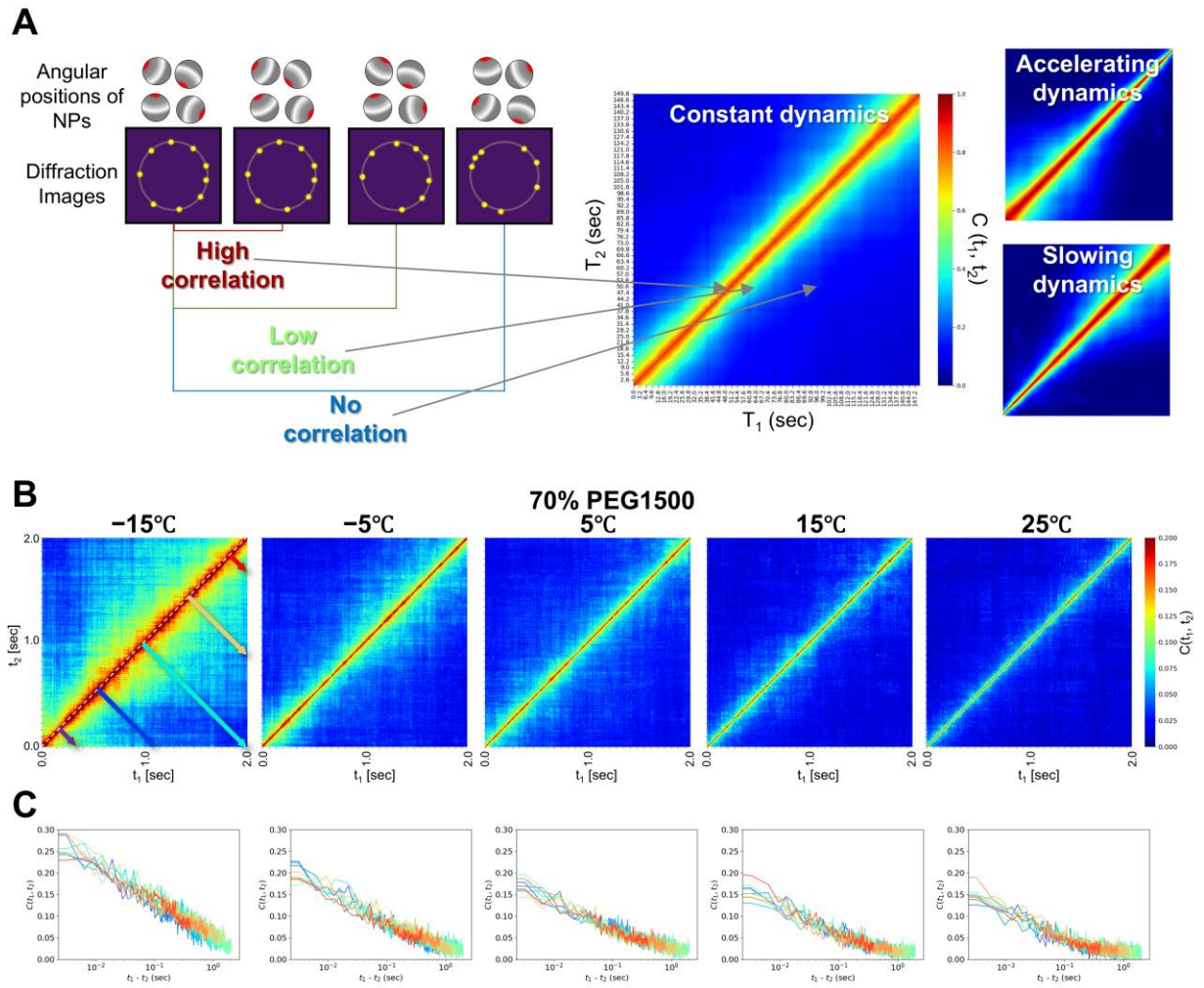


Figure 4. Evaluation of X-ray induced damage for 70% PEG1500 solution by using TTC analysis of ZnO diffraction intensity. (A) Schematic interpretation of TTC. Left: The correlation value $C(t_1, t_2)$ reflects the similarity between diffraction patterns at different times, indicating the similarity in the angular orientation of ZnO NPs. As the lag ($t_1 - t_2$) increases, $C(t_1, t_2)$ gradually decreases. Right: Three example TTC heatmaps illustrating constant, accelerating, and decelerating dynamics. (B) Comparison of TTC maps for 70% PEG1500 solution at different temperatures. (C) Diagonal cuts extracted from the TTC map as indicated by arrows in (B). Each curve was extracted 200 ms intervals.

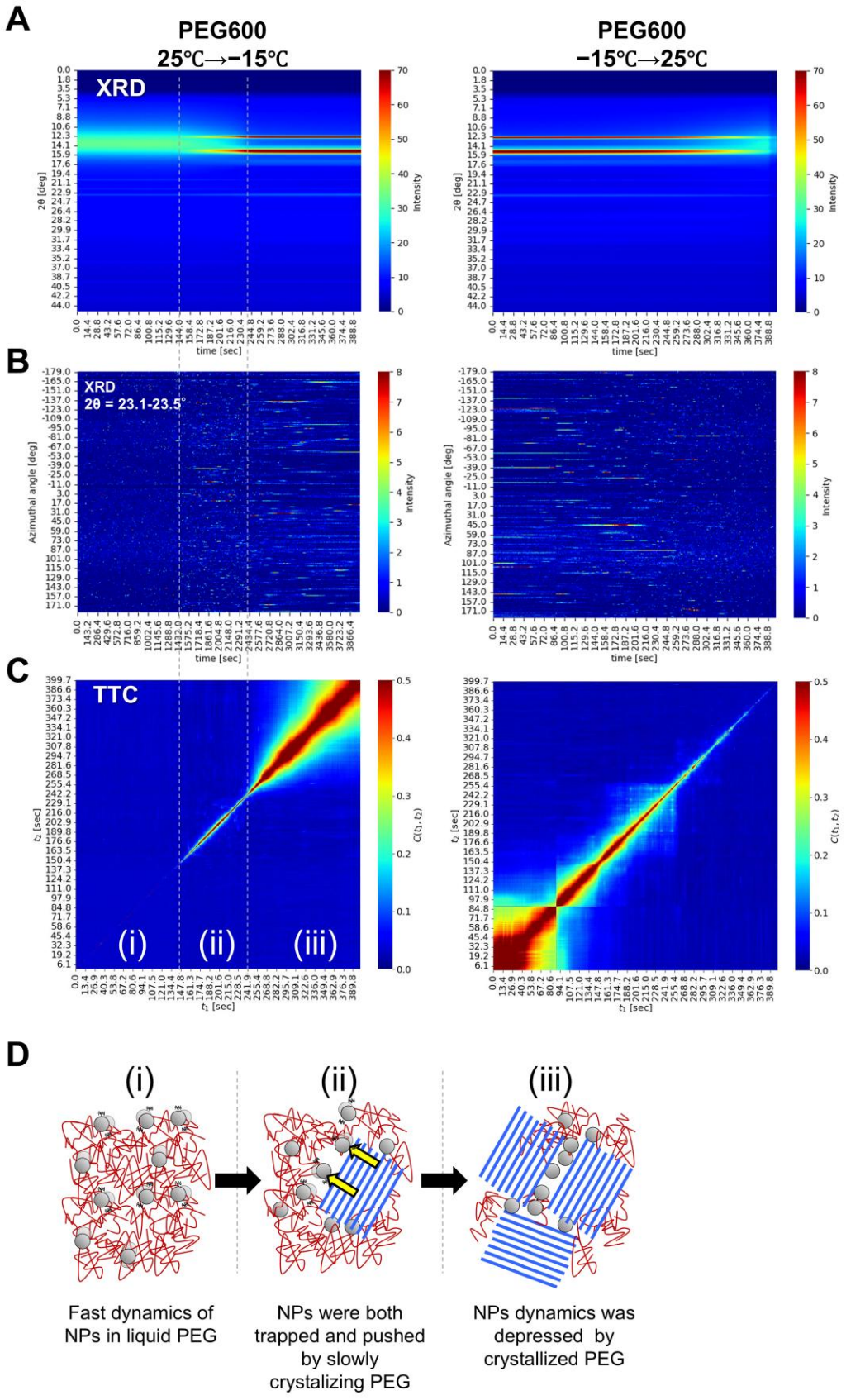

A
PEG600
25℃→−15℃
PEG600
−15℃→25℃
XRD
2θ [deg]
time [sec]
Intensity
B
XRD
2θ = 23.1-23.5°
Azimuthal angle [deg]
time [sec]
Intensity
C
TTC
(i)
(ii)
(iii)
t_2 [sec]
t_1 [sec]
$C(t_1, t_2)$
D
(i)
(ii)
(iii)
Fast dynamics of NPs in liquid PEG
NPs were both trapped and pushed by slowly crystalizing PEG
NPs dynamics was depressed by crystallized PEG

Figure 5. XRD and TTC analysis of ZnO NPs in PEG600 during temperature-induced phase transitions. (A) Two-dimensional heatmap of XRD intensity plotted as a function of 2θ (y-axis) and time (x-axis). (B) Two-dimensional heatmap of XRD intensity as a function of azimuthal angle (φ) and time, extracted from the ZnO (101) diffraction region (2θ = 23.1°–23.5°). (C) TTC heatmaps of ZnO in PEG600 during cooling (left) and heating (right). (D) Schematic illustration of NP motion during cooling process of PEG600. Stages (i)-(iii) correspond to those in (C).

Supporting Information.

Supporting Information: Detailed methods of sample preparation, X-ray diffraction measurement, DXB and TTC analyses, and additional experimental data (DOC).

AUTHOR INFORMATION

Corresponding Author

Email: t.arai@elms.hokudai.ac.jp

Tel: +81-11-706-2770

Address: Laboratory of Protein Science, Department of Advanced Transdisciplinary Sciences, Hokkaido University, N10, W8, Kita-ku, Sapporo, Hokkaido, 060-0810, Japan

Author Contributions

Tatsuya Arai and Yuji C. Sasaki designed the research. Tatsuya Arai, Masahiro Kuramochi, and Daisuke Sasaki prepared the sample. Tatsuya Arai, Masahiro Kuramochi, Daisuke Sasaki, Kazuhiro Mio, Hiroshi Sekiguchi, and Yuji C. Sasaki conducted the X-ray diffraction measurement. Tatsuya Arai, Masahiro Kuramochi, Sakae Tsuda, Daisuke Sasaki, and Yuji C. Sasaki analyzed the data. Kazuhiro Mio, Hiroshi Sekiguchi, and Tomoyasu Aizawa aided in interpreting the results. Tatsuya Arai and Sakae Tsuda wrote the initial manuscript. All authors have read and discussed the manuscript and agreed to its final version for publication.

Funding Sources

This work was supported by JST, ACT-X Grant Number JPMJAX23D2, Japan.

ACKNOWLEDGMENT

The DXB experiments were performed at BL40XU in SPring-8, Japan (under the Approval No. 2022A1308, 2022B1251, 2023A1147, 2024A1102, and 2024B1160).

ABBREVIATIONS

ACF, autocorrelation function; DLS, dynamic light scattering; DXB, diffracted X-ray blinking; DXT, diffracted X-ray tracking; FCS, fluorescence correlation spectroscopy; GI, grazing incidence; NP, nanoparticle; PNC, polymer nanocomposite; PVA, polyvinyl alcohol; SAXS, small-angle X-ray scattering; SPT, single particle tracking; TTC, two-time correlation; vNR, vulcanized natural rubber; WAXD, wide-angle X-ray diffraction; XPCS, X-ray photon correlation spectroscopy.

REFERENCES

[1] S.C. Tjong, Structural and mechanical properties of polymer nanocomposites, Materials Science and Engineering: R: Reports 53 (2006) 73–197. https://doi.org/10.1016/j.mser.2006.06.001.

[2] Q. Wang, L. Zhu, Polymer nanocomposites for electrical energy storage, J Polym Sci B Polym Phys 49 (2011) 1421–1429. https://doi.org/10.1002/polb.22337.

[3] Z. Han, A. Fina, Thermal conductivity of carbon nanotubes and their polymer nanocomposites: A review, Prog Polym Sci 36 (2011) 914–944. https://doi.org/10.1016/j.progpolymsci.2010.11.004.

[4] A.E. Imel, S. Rostom, W. Holley, D. Baskaran, J.W. Mays, M.D. Dadmun, The tracer diffusion coefficient of soft nanoparticles in a linear polymer matrix, RSC Adv 7 (2017) 15574–15581. https://doi.org/10.1039/C7RA00871F.

[5] J. Park, E.J. Bailey, R.J. Composto, K.I. Winey, Single-Particle Tracking of Nonsticky and Sticky Nanoparticles in Polymer Melts, Macromolecules 53 (2020) 3933–3939. https://doi.org/10.1021/acs.macromol.0c00457.

[6] K.A. Rose, M. Molaei, M.J. Boyle, D. Lee, J.C. Crocker, R.J. Composto, Particle tracking of nanoparticles in soft matter, J Appl Phys 127 (2020) 191101. https://doi.org/10.1063/5.0003322.

[7] P.C. Cai, B.A. Krajina, M.J. Kratochvil, L. Zou, A. Zhu, E.B. Burgener, P.L. Bollyky, C.E. Milla, M.J. Webber, A.J. Spakowitz, S.C. Heilshorn, Dynamic light scattering microrheology for soft and living materials, Soft Matter 17 (2021) 1929–1939. https://doi.org/10.1039/D0SM01597K.

[8] D. Wöll, Fluorescence correlation spectroscopy in polymer science, RSC Adv 4 (2014) 2447–2465. https://doi.org/10.1039/C3RA44909B.

[9] F. Lehmkühler, W. Roseker, G. Grübel, From Femtoseconds to Hours—Measuring Dynamics over 18 Orders of Magnitude with Coherent X-rays, Applied Sciences 11 (2021) 6179. https://doi.org/10.3390/app11136179.

[10] J. Carnis, W. Cha, J. Wingert, J. Kang, Z. Jiang, S. Song, M. Sikorski, A. Robert, C. Gutt, S.-W. Chen, Y. Dai, Y. Ma, H. Guo, L.B. Lurio, O. Shpyrko, S. Narayanan, M. Cui, I. Kosif, T. Emrick, T.P. Russell, H.C. Lee, C.-J. Yu, G. Grübel, S.K. Sinha, H. Kim, Demonstration of Feasibility of X-Ray Free Electron Laser Studies of Dynamics of Nanoparticles in Entangled Polymer Melts, Sci Rep 4 (2014) 6017. https://doi.org/10.1038/srep06017.

[11] A. Madsen, A. Fluerasu, B. Ruta, Structural Dynamics of Materials Probed by X-Ray Photon Correlation Spectroscopy, in: Synchrotron Light Sources and Free-Electron Lasers, Springer International Publishing, Cham, 2015: pp. 1–21. https://doi.org/10.1007/978-3-319-04507-8_29-1.

[12] H. Sekiguchi, M. Kuramochi, K. Ikezaki, Y. Okamura, K. Yoshimura, K. Matsubara, J.W. Chang, N. Ohta, T. Kubo, K. Mio, Y. Suzuki, L.M.G. Chavas, Y.C. Sasaki, Diffracted X-ray Blinking Tracks Single Protein Motions, Sci Rep 8 (2018) 6–13. https://doi.org/10.1038/s41598-018-35468-3.

[13] T. Arai, R. Inamasu, H. Yamaguchi, D. Sasaki, A. Sato-Tomita, H. Sekiguchi, K. Mio, S. Tsuda, M. Kuramochi, Y.C. Sasaki, Laboratory diffracted x-ray blinking to monitor picometer motions of protein molecules and application to crystalline materials, Structural Dynamics 8 (2021) 044302. https://doi.org/10.1063/4.0000112.

[14] M. Kuramochi, Y. Dong, Y. Yang, T. Arai, R. Okada, Y. Shinkai, M. Doi, K. Aoyama, H. Sekiguchi, K. Mio, S. Tsuda, Y.C. Sasaki, Dynamic motions of ice-binding proteins in living Caenorhabditis elegans using diffracted X-ray blinking and tracking, Biochem Biophys Rep 29 (2022) 101224. https://doi.org/10.1016/j.bbrep.2022.101224.

[15] J. Chang, T. Arai, M. Kuramochi, R. Inamasu, Z. Lee, T. Ohkubo, K. Mio, Y.C. Sasaki, Dynamic observations of various oligomers in amyloid β isoforms using laboratory

diffracted X-ray blinking, Biochem Biophys Rep 31 (2022) 101298. https://doi.org/10.1016/j.bbrep.2022.101298.

[16] M. Kuramochi, H. Omata, M. Ishihara, S. Hanslin, M. Mizumaki, N. Kawamura, H. Osawa, M. Suzuki, K. Mio, H. Sekiguchi, Y.C. Sasaki, Tilting and rotational motions of silver halide crystal with diffracted X-ray blinking, Sci Rep 11 (2021) 1–9. https://doi.org/10.1038/s41598-021-83320-y.

[17] R. Inamasu, H. Yamaguchi, T. Arai, J. Chang, M. Kuramochi, K. Mio, Y.C. Sasaki, Observation of molecular motions in polymer thin films by laboratory grazing incidence diffracted X-ray blinking, Polym J 55 (2023) 703–709. https://doi.org/10.1038/s41428-023-00762-z.

[18] M. Kuramochi, H.J. Kirkwood, J.C.P. Koliyadu, R. Letrun, R. de Wijn, C. Kim, T. Masui, K. Mio, T. Arai, H. Sekiguchi, H. Kishimoto, A.P. Mancuso, T. Sato, Y.C. Sasaki, Direct observation of 890 ns dynamics of carbon black and polybutadiene in rubber materials using diffracted x-ray blinking, Appl Phys Lett 123 (2023) 101601. https://doi.org/10.1063/5.0157359.

[19] D. Dash, C. Mallika, U. Kamachi Mudali, Temperature and Concentration Dependence of Viscosity of Binary Mixtures of PEG-1000 + water, Chemical Product and Process Modeling 12 (2017) 20160037. https://doi.org/10.1515/cppm-2016-0037.

[20] K. Koga, A. Takada, N. Nemoto, Dynamic Light Scattering and Dynamic Viscoelasticity of Poly(vinyl alcohol) in Aqueous Borax Solutions. 5. Temperature Effects, Macromolecules 32 (1999) 8872–8879. https://doi.org/10.1021/ma990493w.

[21] Y. Shinohara, N. Yamamoto, H. Kishimoto, Y. Amemiya, X-ray irradiation induces local rearrangement of silica particles in swollen rubber, J Synchrotron Radiat 22 (2015) 119–123. https://doi.org/10.1107/S1600577514022954.

[22] M. Sutton, K. Laaziri, F. Livet, F. Bley, Using coherence to measure two-time correlation functions, Opt Express 11 (2003) 2268. https://doi.org/10.1364/OE.11.002268.

[23] A. Ragulskaya, V. Starostin, F. Zhang, C. Gutt, F. Schreiber, On the analysis of two-time correlation functions: equilibrium versus non-equilibrium systems, J Appl Crystallogr 57 (2024) 1098–1106. https://doi.org/10.1107/S1600576724004618.

[24] R. Paberit, E. Rilby, J. Göhl, J. Swenson, Z. Refaa, P. Johansson, H. Jansson, Cycling Stability of Poly(ethylene glycol) of Six Molecular Weights: Influence of Thermal Conditions for Energy Applications, ACS Appl Energy Mater 3 (2020) 10578–10589. https://doi.org/10.1021/acsaem.0c01621.

[25] T. Hoshino, Y. Okamoto, A. Yamamoto, H. Masunaga, Heterogeneous dynamics in the curing process of epoxy resins, Sci Rep 11 (2021) 9767. https://doi.org/10.1038/s41598-021-89155-x.

[26] T. Hoshino, Y. Okamoto, A. Yamamoto, H. Masunaga, Dynamic behaviours of epoxy resin thin films during the curing process, Soft Matter 19 (2023) 3267–3272. https://doi.org/10.1039/D2SM01500E.

[27] A.-C. Genix, J. Oberdisse, Structure and dynamics of polymer nanocomposites studied by X-ray and neutron scattering techniques, Curr Opin Colloid Interface Sci 20 (2015) 293–303. https://doi.org/10.1016/j.cocis.2015.10.002.

[28] E.J. Bailey, K.I. Winey, Dynamics of polymer segments, polymer chains, and nanoparticles in polymer nanocomposite melts: A review, Prog Polym Sci 105 (2020) 101242. https://doi.org/10.1016/j.progpolymsci.2020.101242.

[29] K. Mio, T. Ohkubo, D. Sasaki, M. Sugiura, K. Kawaguchi, K. Araki, K. Taninaka, M. Sakaguchi, S. Nozawa, T. Arai, Y.C. Sasaki, Simultaneous Recording of Remote Domain Dynamics in Membrane Proteins Using the Double-Labeled DXB/DXT Technique, Membranes (Basel) 14 (2024) 75. https://doi.org/10.3390/membranes14040075.

[30] N.N. Striker, I. Lokteva, M. Dartsch, F. Dallari, C. Goy, F. Westermeier, V. Markmann, S.C. Hövelmann, G. Grübel, F. Lehmkühler, Dynamics and Time Scales of Higher-Order Correlations in Supercooled Colloidal Systems, J Phys Chem Lett 14 (2023) 4719–4725. https://doi.org/10.1021/acs.jpclett.3c00631.

[31] Z. Hu, J.J. Donatelli, J.A. Sethian, Cross-correlation analysis of X-ray photon correlation spectroscopy to extract rotational diffusion coefficients, Proceedings of the National Academy of Sciences 118 (2021). https://doi.org/10.1073/pnas.2105826118.

[32] L. Cristofolini, D. Orsi, L. Isa, Characterization of the dynamics of interfaces and of interface-dominated systems via spectroscopy and microscopy techniques, Curr Opin Colloid Interface Sci 37 (2018) 13–32. https://doi.org/10.1016/j.cocis.2018.06.001.

[33] Y.C. Sasaki, Y. Okumura, S. Adachi, Y. Suzuki, N. Yagi, Diffracted X-ray tracking: New system for single molecular detection with X-rays, Nucl Instrum Methods Phys Res A 467–468 (2001) 1049–1052. https://doi.org/10.1016/S0168-9002(01)00717-3.

For Table of Contents Only

